Available online at www.sciencedirect.com
SCIENCE DIRECT®
Journal of Power Sources 145 (2005) 610–619
JOURNAL OF POWER SOURCES
www.elsevier.com/locate/jpowsour

Experimental study of a fuel cell power train for road transport application

P. Corbo *, F.E. Corcione, F. Migliardini, O. Veneri

Istituto Motori, Italian National Research Council, Via G.Marconi 8, 80125 Napoli, Italy

Accepted 7 February 2005
Available online 29 April 2005

Abstract

The development of fuel cell electric vehicles requires the on-board integration of fuel cell systems and electric energy storage devices, with an appropriate energy management system. The optimization of performance and efficiency needs an experimental analysis of the power train, which has to be effected in both stationary and transient conditions (including standard driving cycles).

In this paper experimental results concerning the performance of a fuel cell power train are reported and discussed. In particular characterization results for a small sized fuel cell system (FCS), based on a 2.5 kW PEM stack, alone and coupled to an electric propulsion chain of 3.7 kW are presented and discussed. The control unit of the FCS allowed the main stack operative parameters (stoichiometric ratio, hydrogen and air pressure, temperature) to be varied and regulated in order to obtain optimized polarization and efficiency curves. Experimental runs effected on the power train during standard driving cycles have allowed the performance and efficiency of the individual components (fuel cell stack and auxiliaries, dc–dc converter, traction batteries, electric engine) to be evaluated, evidencing the role of output current and voltage of the dc–dc converter in directing the energy flows within the propulsion system.

Keywords: PEM fuel cells; Power train; Electric vehicles; Energy management

1. Introduction

Air pollution, oil dependence and greenhouse gas emissions are persistent problems for gasoline and diesel vehicles, although improvements of conventional engine technologies have partially mitigated these problems, and further refinements could provide additional progress in the future. While hybrid gasoline–electric vehicles are emerging as a promising option, the alternative of the pure electric vehicles have been proposed in recent years with the aim of decoupling oil from transportation sector with zero local emissions. However, the limitations of electric vehicles equipped with traditional energy storage systems justify the strong research interest for new solutions able to improve the vehicle range, and to reduce battery recharging time, maintaining the crucial advantage of local zero emissions. In this context fuel cells could become, in a not-too-distant future, a primary source of power for automotive applications, thanks to their high efficiency and capability to use hydrogen as fuel without generating pollutant emissions [1–4]. The polymeric exchange membrane (PEM) fuel cells are the most likely candidate for automotive applications, due to their high power density and low operative temperature (60–90 °C), with consequent fast start-up, good dynamic behavior and reliable service if fuelled by pure hydrogen [5,6].

The utilization of fuel cells in a propulsion system for road transport application generates the question of which is the optimal hybridization level between on board generation and storage of electric energy (batteries, supercapacitors). In particular, the fuel cell system can be integrated in the propulsion system either as load following or load leveled power source. In the first case the storage system to be used is minimized, and the fuel cell stack generates all the energy demanded by

* Corresponding author.
E-mail address: p.corbo@im.cnr.it (P. Corbo).

0378-7753/$ – see front matter © 2005 Elsevier B.V. All rights reserved.
doi:10.1016/j.jpowsour.2005.02.054

the load, with the only limitation determined by dynamics of the stack. In the second option the power provided by the fuel cell is limited, and the peak energy requirements are satisfied by the storage system. The main benefit of the load following configuration is the minor use of the batteries, which could have the minimum capacity necessary to feed the vehicle auxiliaries and allow some energy economy during regenerative braking. On the other hand, the load leveled option offers the possibility to use a smaller fuel cell stack, which can work in optimal efficiency conditions, while a major use of batteries is necessary, in order to provide peak powers, and to recover some of energy lost during braking. Some published results, based on simulation programs [7], have shown that the regenerative breaking can have a strong effect on the energy consumption of a fuel cell propulsion system, in particular for small power systems and less demanding driving cycles.

This paper reports the experimental results obtained on a fuel cell propulsion system designed for a moped and installed on a test bench. It utilizes a 2.5 kW PEM fuel cell stack, 3.7 kW maximum power electrical drive and a lead-acid battery pack as storage system. The results, obtained on two different driving cycles (European R40 and R47), have provided indications about the power train efficiency, and on the main issues of energy management to be dealt with for directing energy flows within the system.

2. Experimental

The experimental runs were performed on a laboratory plant constituted by the following components: fuel cell system, dc–dc converter, electrical energy storage system, electrical drive coupled to a braking electrical machine, data acquisition systems. In the following, some details on the different subsystems and on the issues related to the integration of all components in the overall propulsion chain are given.

Table 1
Technical specifications of the Proton Motor fuel cell system (FCS)

Electric output	Maximum 2 kW after dc–dc converter
Dynamic	Maximum change rate 500 W s^{-1}
Hydrogen	
Purity	99.999% H_2
FCS inlet gas pressure	500 kPa
FCS inlet gas stream	At least 3 N m^3 h^{-1}
Nitrogen	
Purity	99.999% N_2
FCS inlet gas pressure	500 kPa
FCS inlet gas stream	At least 1 N m^3 h^{-1}
Maximum stack temperature	<343 K
Communication	Ethernet/TCP IP
Maximum cooling water in	333 K
Small battery maximum current output 12 V	10 A
Small battery maximum recharging current	4 A
Air compressor	Side channel, 24 V dc, maximum pressure16 kPa
Water pump (cooling and humidification)	Circulating pump, 24 V dc, 20 kPa, 7 l min^{-1}

2.1. The fuel cell system

The fuel cell system, realized by PROTON MOTOR Fuel Cell GmbH, is based on a 2.5 kW PEM stack fuelled with pure hydrogen at low pressure (25–40 kPa, dead-end operation), and comprises all the auxiliary components necessary to the fuel cell operation, such as air supply unit, fuel supply unit, cooling system, humidification system and fuel cell control system. In Table 1 the technical specifications of the system are reported, while a scheme of the overall apparatus is shown in Fig. 1.

Hydrogen was supplied by cylinders at 200 bar inserted in the laboratory decompression unit, while a side channel compressor was used to feed air to the stack. The cooling system was constituted by a de-ionized water circuit equipped

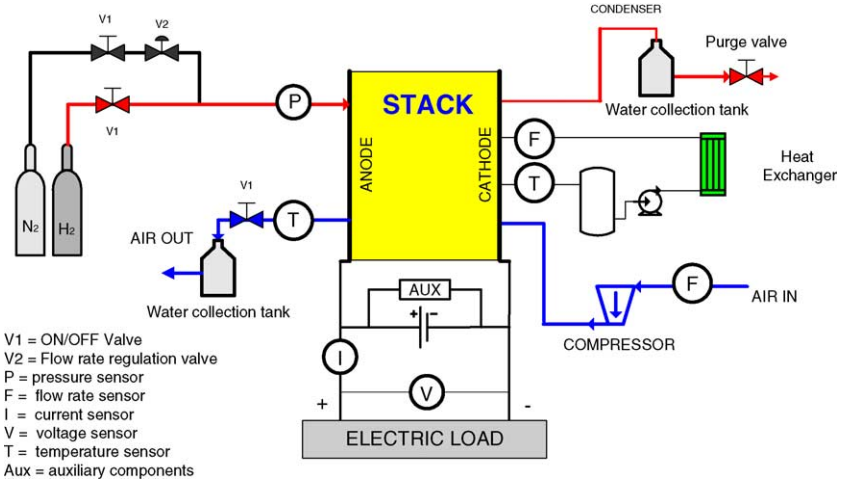

Fig. 1. Scheme of the fuel cell system experimental apparatus.

Table 2
Technical characteristics of the electrical drive

Type	Brushless
Maximum power	3.7 kW
Rated current	32 A
Maximum current	100 A
Link voltage	48 V
Motor voltage	35 V
2p	4
Rated speed	3000 rpm
Maximum speed	6000 rpm

by pump, temperature and flow rate sensors. A heat exchanger fed with external water was used to control the cooling water temperature.

Stack humidification was assured by injection of deionized water into the inlet air manifold. The injection was automatically activated when outlet air temperature overcame 60 °C.

National Instruments FieldPoint devices were used to acquire the signals produced by all sensors (output air, output water temperature, inlet air flow rate, inlet hydrogen pressure, output total current and voltage) and to control the overall system.

A small 24 V lead-acid battery was added to the system in order to permit the start up of all auxiliary components before starting of the fuel cell.

2.2. The electrical drive

The technical specifications of the electrical drive used in the propulsion system are reported in Table 2.

A LAFERT brushless engine of 3.7 kW maximum power was used, of the same typology of that installed on electrical commercial mopeds. Its characteristic curves are reported in Fig. 2 in terms of power and torque versus revolution speed. This engine was equipped with a controlled inverter and was coupled to an eddy current braking machine. Being the engine to wheel speed ratio fixed it was possible to reproduce vehicle inertia by means of an equivalent flywheel, while aerodynamic drag and rolling resistance were performed by

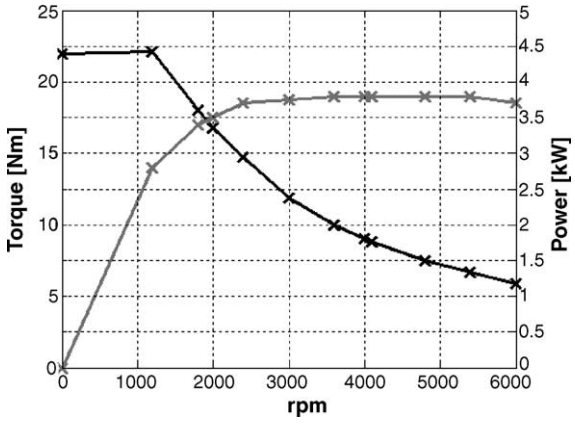

Fig. 2. Characteristic curves of the electric engine.

Table 3
Technical specifications of the dc–dc converter

Maximum inlet voltage	34 V
Minimum inlet voltage	19 V
Rated inlet voltage	24 V
Rated output voltage	48 V (±1%)
Rated power	2.8 kW
Rated efficiency	86%

the eddy current brake. This system allowed to effect different driving cycles, implemented by a control software specifically developed. A lead-acid battery pack of 4 units, each one of 12 V and 38 Ah, was used as electrical energy storage system. The choice of the best storage system was not the main goal of this paper, then lead-acid batteries were adopted as they are a standard product characterized by low cost and good efficiency.

2.3. The fuel cell propulsion system

The stack output voltage ranged from 34 V at open circuit to 22 V at full load, while the electrical engine required electric current at 48 V dc, then a dc–dc converter was necessary to match the stack output voltage to that required by the engine. In Table 3 the technical specification of the dc–dc converter are shown. The electric connections used for experimental tests on the overall fuel cell propulsion system are shown in Fig. 3. Downstream of the converter a dc bus permitted the connection between converter, battery pack and load. The energy flow was unidirectional from stack toward dc bus, while the battery pack could be recharged by both stack and engine (during regenerative braking) and discharged when the energy required from the engine is higher than the energy provided by the fuel cell system.

LEM voltage and current sensors were installed on batteries, and upstream–downstream the dc–dc converter (Fig. 3), to monitor the electric energy flows between the different components of the propulsion system. The dc–dc converter is a critical component in the energy flow management within the propulsion system, in particular allows the stack output power to be varied according to the selected control strategy. This variation was performed by manual regulation of voltage and current reference at the device output.

Furthermore, some security switches were adopted, in order to instantaneously disconnect the electric load from battery pack and/or stack.

An I/O laboratory board was used for data acquisition and setting of the electrical parameter affecting the dc–dc converter behavior.

3. Efficiency calculations

The experimental results reported in the present paper allowed efficiency evaluations to be effected, on both the fuel cell system alone and the overall propulsion system.

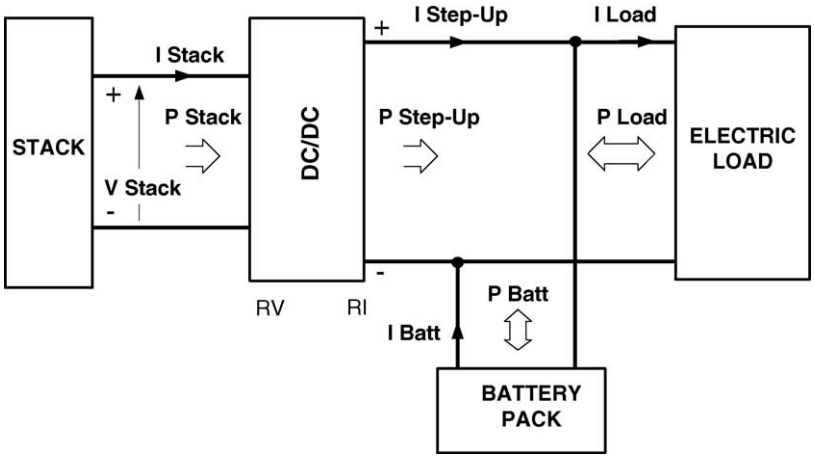

Fig. 3. Electric connections between stack, batteries and load.

The stack efficiency was calculated by the following equation:

$$\eta_{\text{stack}} = \frac{V}{V_{\text{id}}} \tag{1}$$

where V is the measured output stack voltage and V_{id} is the reversible open circuit stack voltage (1.23 V), given by $-\Delta G_{\text{f}}/2F$. Here ΔG_{f} is the Gibbs free energy of formation in the normal state for the reaction $H_2 + 1/2O_2 = H_2O$, while F is the Faraday constant. The thermodynamic efficiency (η_{therm}) is defined by the ratio of ΔG_{f} to ΔH_{f}, which is the lower heating value for hydrogen combustion. The value of this efficiency is 98% at 298 K.

During stack operation a partial hydrogen purge is necessary, then it is possible to define a fuel utilization efficiency (η_{util}) as ratio between mass of fuel reacted in the stack and mass of fuel entering the stack. It was experimentally estimated in three steady state conditions (500, 1000 and 1500 W of stack power), being known the opening time of the anode purge valve and measuring opening frequency and purged volume. The coefficient resulted equal to 0.98 in the three conditions examined, and this value was assumed valid also during transient tests.

The efficiency losses due to all auxiliary components (air compressor, water pump, cable resistance, other electrical minor components) necessary to stack operation can be taken into account by an experimental coefficient (η_{abs}) expressed as ratio between power at dc–dc converter inlet and stack power.

The total efficiency of the fuel cell system can be then calculated by the following equation:

$$\eta_{\text{FCS}} = \eta_{\text{therm}}\eta_{\text{util}}\eta_{\text{stack}}\eta_{\text{abs}} \tag{2}$$

and expresses the ratio between the power at dc–dc converter input and the theoretical power associated to the fuel entering the stack.

The experimental determination of dc–dc converter (η_{dc}) and electrical drive (η_{ED}) efficiency was also performed. Both were calculated as ratio between outlet and inlet power of the devices.

The electrochemical efficiency of storage batteries is defined as ratio between the integral of the instantaneous current during a discharge and the same integral during a charge, if the status of the battery before and after the calculation is the same:

$$\eta_{\text{batt}} = \frac{\int_0^{t_{\text{d}}} I_{\text{d}}\,\text{d}t}{\int_0^{t_{\text{c}}} I_{\text{c}}\,\text{d}t}$$

where I_{d}, and I_{c} are the battery current during the discharge and charge periods, respectively, while t_{d} and t_{c} are the lengths of these periods. The determination of this efficiency for a specific type and sample of battery, with reference to a particular driving cycle, requires the experimental evaluation of the battery state of charge (SOC), which is based on specific tests which are beyond the scope of this paper [8]. On the other hand, for lead-acid batteries, used in the present work, it has been experimentally verified that very low energy losses can be detected if charge and discharge operations are very fast, in particular in short cycles of charge and discharge (about 30 min) an energy efficiency higher than 92% has been obtained [9]. Since in the experiments presented in this paper the single periods of charge and discharge of the battery pack last not more of two minutes, and current involved was higher than 10 A only during the fast acceleration phase of the R47 cycle (see Section 4.2), a value of 100% for the battery energy efficiency was assumed valid in all tests. On this hypothesis it is possible to define the battery state of charge as:

$$\text{SOC}(t) = \text{SOC}^0 + \int_{t^0}^{t} I_{\text{batt}}(t)\text{d}t \tag{3}$$

where SOC^0 is the known battery state of charge at the time t^0. This definition is utilized in this paper to instantaneously calculate the battery SOC during the driving cycles, starting from the experimental measurements of battery current and voltage.

Finally the total efficiency of the power train on the driving cycle is defined by the following equation:

$$\eta_{PT} = \frac{E_{load}}{E_{H_2} + E_{batt}} \quad (4)$$

where

$$E_{batt} = \int_{t_1}^{t_2} V_{batt} I_{batt} dt, \qquad E_{load} = \int_{t_1}^{t_2} T_m \omega_m dt,$$

$$E_{H_2} = \frac{1}{\eta_{util}} \int_{t_1}^{t_2} M_{H_2} n_{cells} I \frac{\Delta H_f}{2F} dt$$

where V_{batt} is the battery voltage, I_{batt} the battery current, T_m the brake torque, ω_m the engine speed, M_{H_2} the hydrogen molecular weight, n_{cells} the cell number, I the stack current, E_{load} the energy provided by the , while E_{H_2} is the energy coming from hydrogen and E_{batt} is the net energy exchanged by the battery pack during the cycle.

4. Results and discussion

In order to elucidate the contribution of different components of the propulsion system in determining the global efficiency, the experimental runs were firstly oriented to the characterization of the fuel cell system, determining the energy losses associated to its working in steady state conditions. The efficiency of the single components and of the overall power train was then determined on two different driving cycles (European R40 and R47).

4.1. Fuel cell system characterization

In Fig. 4 the characteristic curves of the 2.5 kW stack are reported, in terms of voltage and power versus stack current. The tests were performed at temperature of 60 °C, hydrogen pressure ranging from 20 to 50 kPa, air pressure from 10 to 16 kPa, stoichiometric ratio (R) ranging 2–6 ($R = R_{eff}/R_{stoich}$ where R_{eff} is the ratio between the air and hydrogen flow rates actually used in the experiments, while R_{stoich} is the same ratio as required by the stoichiometric equation of H_2 oxidation).

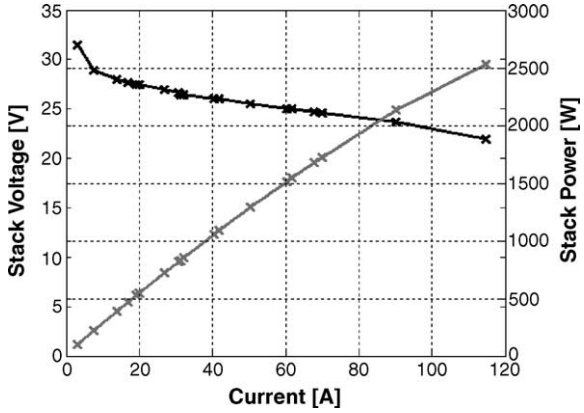

Fig. 4. Stack characteristic curves ($R = 2$–6, $T = 333$ K, $P_{H_2} < 50$ kPa, $P_{air} < 20$ kPa).

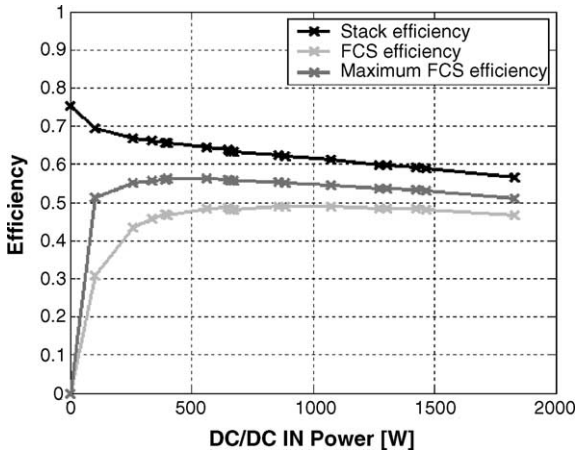

Fig. 5. Efficiency of stack and fuel cell system vs. dc–dc converter inlet power. Experimental conditions of Fig. 4.

The output voltage decreases from 32 V at low load to about 22 V at the highest load tested (115 A), while at this load the power curve reaches the peak value of 2.5 kW. In particular, the polarization curve presents a linear relationship between voltage and current in the range 10–90 A, with a voltage decrease from 27 to 24 V. In Fig. 5 the stack efficiency curve (η_{stack}) is plotted against the power produced by the fuel cell system, which was measured at the dc–dc converter inlet. The efficiency varies from 0.7 at 100 W to 0.56 at 1.8 kW of FCS power. In the same figure, the global efficiency values (η_{FCS}) of the fuel cell system are also reported as calculated by Eq. (2). These values represent the ratio between the power entering the dc–dc converter and the power entering the stack in form of hydrogen flow rate. Due to the different causes of energy loss inside the system the global efficiency does not overcome 50%. The details of these energy losses are exploited in Fig. 6, where the absorbed power of different components of the fuel cell system are reported as function of

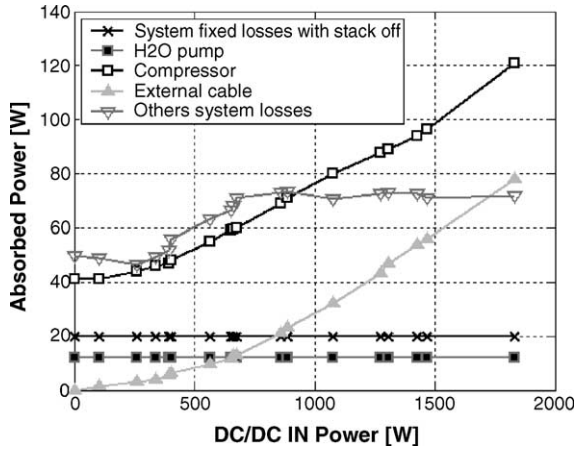

Fig. 6. Power losses associated to the main fuel cell system components vs. dc–dc converter inlet power Experimental conditions of Fig. 4.

the power entering the dc–dc converter. It can be observed that the major energy consumption is due to the air compressor (about 120 W at 1.8 FCS power), while minor losses are associated to the cooling and humidification water pumps (about 10 W for each one, constant with respect to load). Further consumptions are due to the electrical external cable used to connect the FCS to the dc–dc converter (about 80 W at maximum load), to undetermined system losses, about 20 W when stack is OFF, and about 70 W with stack ON (several electrical components, which are present in a fuel cell system designed for laboratory tests, such as sensors, electric valves, internal cables, relays, control system boards). The consumption of these last components could be partially reduced, in particular if the fuel cell system were specifically designed for a vehicle, while the energy losses due to air and water management system are difficult to further on lower. In order to individuate on the efficiency plot of Fig. 5, a region in which the behavior of a real fuel cell system could be located, a third efficiency curve (maximum total efficiency) was calculated and reported, considering only air compressor, hydrogen purge and water pump as losses sources. In this case the efficiency could reach the value of 55% at medium load.

4.2. Power train characterization

The experimental tests on the overall power train were performed having as main objectives the evaluation of efficiency on standard driving cycles and the individuation of the basic energy management strategy necessary to assure proper operation during the selected operative procedure. All runs were carried out maintaining the battery SOC at a reasonable level over all driving cycles without charging from an external source, and recovering braking energy as much as possible.

In Figs. 7 and 8 the two driving cycles utilized are reported, in terms of engine speed versus time. The R47 cycle (Fig. 7) is imposed by European legislation for exhaust emission measurements of mopeds powered by internal combustion engine, and was used here in the absence of a specific legislation regarding electrical mopeds. With reference to the particular electrical drive used in this work, the R47 cycle requires the maximum power in the initial phase up to the maximum speed (6000 rpm), then a period of constant speed of 50 s at maximum speed, a fast deceleration up to 2400 rpm, a second period of constant speed, a final deceleration up to zero speed.

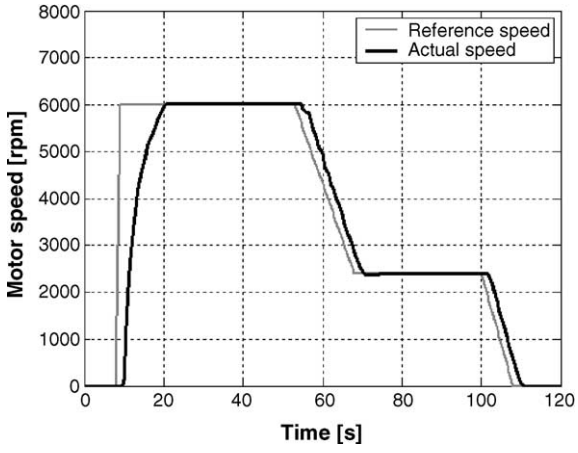

Fig. 7. European driving cycle R47.

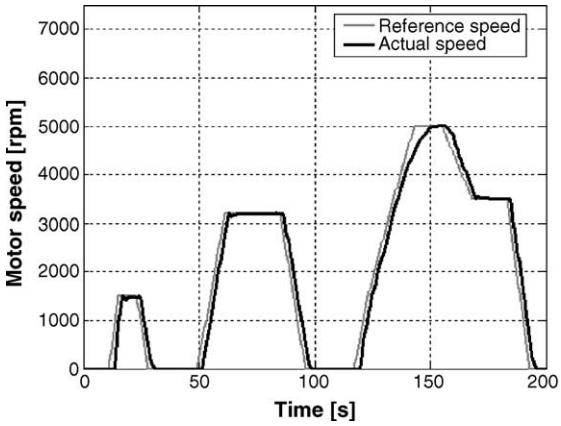

Fig. 8. European driving cycle R40.

The R40 cycle (Fig. 8) is composed by three phases, the first two being characterized by acceleration, constant speed (1500 and 3200 rpm) and deceleration steps, while the last one presents two steps at constant speed (5000 and 3500 rpm), before returning to zero speed. It is required by the European legislation to evaluate the exhaust emissions of motorcycles and, after addition of a fourth phase at higher speed, also for passenger cars. It was used in this work to evaluate the performance of the fuel cell power train on a typical urban route, not strictly associated with the driving way assumed for a moped.

Two test procedures were utilized, the load leveled on the R47 cycle, and load following on the R40 cycle. In each procedure the operating way of the fuel cell system was varied by controlling its output power by regulating of dc–dc converter output voltage and current.

The results of the experimental tests effected on the R47 cycle are reported in Fig. 9a–d. Fig. 9a and b shows the power distribution between FCS, engine, battery pack and dc–dc converter versus cycle length, in comparison with the hydrogen power entering the stack. For this test the energy contribution of the fuel cell system was regulated by imposing a constant voltage reference value at the dc–dc converter output so higher than initial battery voltage to allow the energy flow to be always directed toward load and/or batteries during the cycle length. This reference value, together with the variable battery voltage, are reported in Fig. 9c. The output power of the fuel cell system was fixed at two constant values (900 and 450 W), corresponding to the two phases of the cycle at constant engine speed, by limiting the dc–dc converter output current (Fig. 9a and b). The load following operation could not be adopted for this cycle because the power requirement

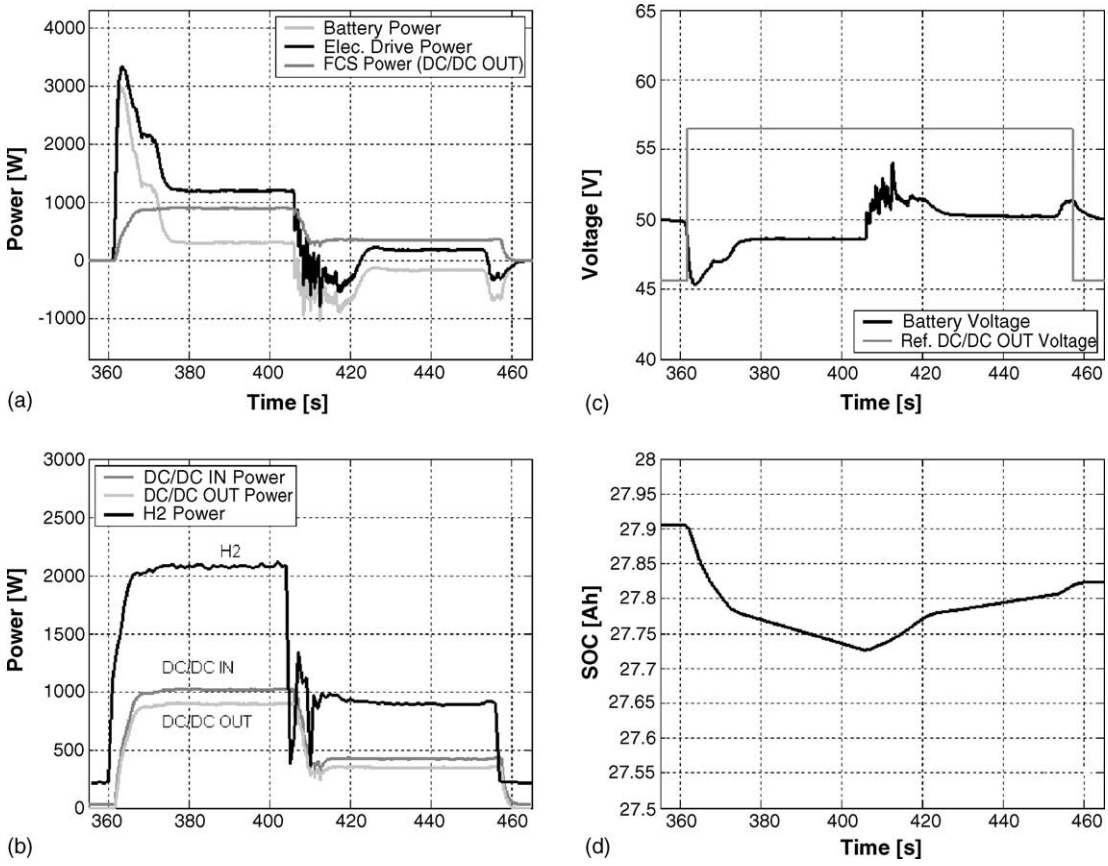

Fig. 9. Experimental results obtained on the fuel cell power train in load leveled configuration on the R47 driving cycle: (a) battery, input electric drive and output dc–dc converter powers vs. cycle length; (b) hydrogen, input and output dc–dc converter powers vs. cycle length; (c) reference dc–dc output voltage and battery voltage powers vs. cycle length; (d) battery state of charge vs. cycle length.

from the engine, especially during the first acceleration phase, was too high with respect to the energy obtainable from the fuel cell system.

The engine power (Fig. 9a) reaches its maximum value (3500 W) during the first acceleration phase, then decreases up to 1200 W corresponding to the first step at constant engine speed, then diminishes up to negative power values during the deceleration phase, when the engine operates as generator. At the end of this deceleration the engine power reaches the second condition of constant speed (220 W), followed by the last deceleration up to zero speed. The battery power curve evidences that the storage system compensates the difference between engine power requirements and the power provided by the fuel cell system (Fig. 9a). In particular the energy flowing from the battery permits the engine power peak to be achieved, while during the regenerative braking, when the motor operates as generator, the battery power drops to negative values indicating a partial energy recovery.

The behavior of battery power affects its state of charge during the cycle, as calculate according to Eq. (3) and shown in Fig. 9d. The highest discharge speed is observed during the first acceleration phase, while the fastest recharging is obtained during the first deceleration, when the batteries are recharged by both engine and stack. During the first constant speed step a slower SOC decrease is observed, while the last two phases of the cycle (second constant speed step and last deceleration) determine the further battery recharging.

Fig. 9b shows the power associated to hydrogen entering the stack, together with the power at the inlet and output dc–dc converter measured during the cycle. The two curves obtained for the converter evidence the energy loss caused by this critical component, while the comparison with the hydrogen power plot visualizes the energy loss associated to the fuel cell system.

The results of the tests performed on the R40 cycle are shown in Fig. 10a–d. Being this cycle characterized by less demanding power requirement during all its phases, it was possible to adopt the load following configuration. Then during these tests the contribution of batteries to the energy requirement coming from the engine was minimized by imposing a voltage reference value at the dc–dc converter output equal to the initial battery voltage, with no current limitation. Fig. 10c evidences the behavior of batteries during this test, in particular their voltage remains close to the reference value during the major part of the cycle length, slightly decreases when the engine requires power, and quickly rises during the short regenerative braking phases. In Fig. 10a engine, battery and dc–dc converter powers versus cycle length are reported,

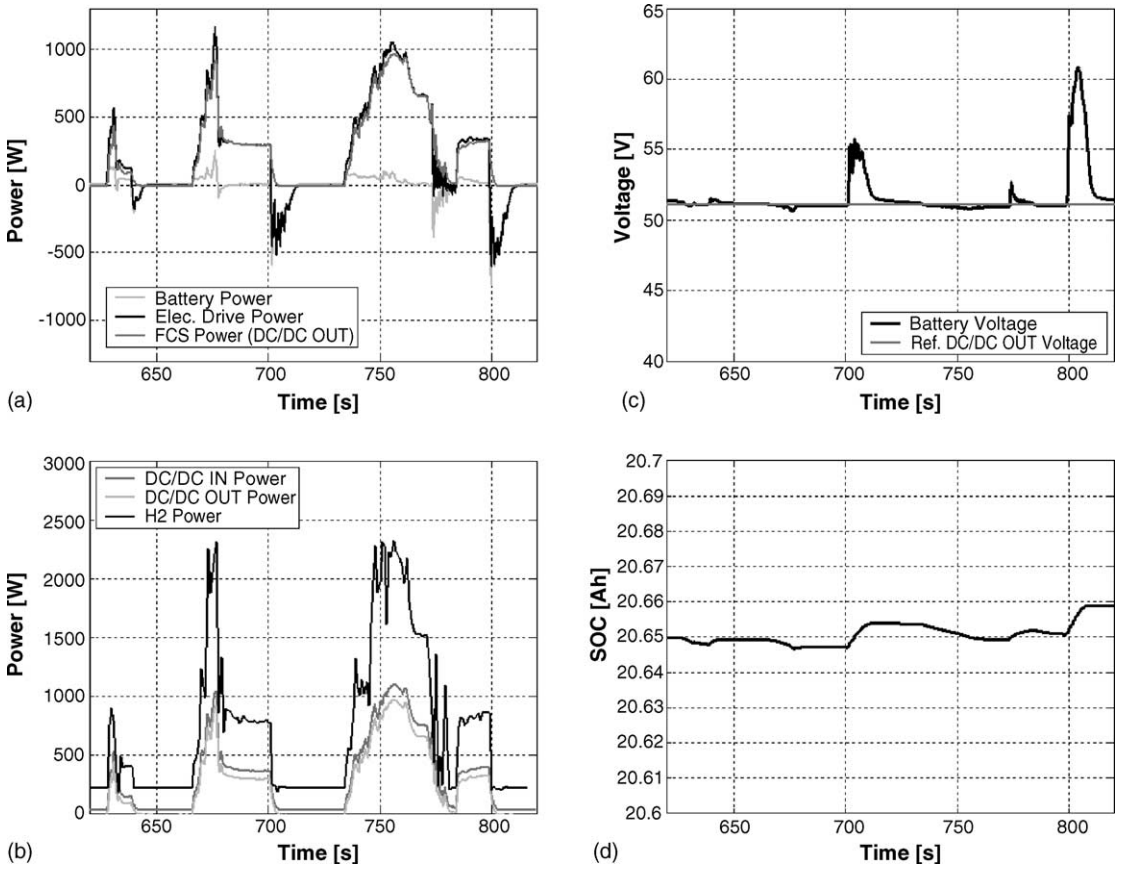

Fig. 10. Experimental results obtained on the fuel cell power train in load following configuration on the R40 driving cycle: (a) battery, input electric drive and output dc–dc converter powers vs. cycle length; (b) hydrogen, input and output dc–dc converter powers vs. cycle length; (c) reference dc–dc output voltage and battery voltage powers vs. cycle length; (d) battery state of charge vs. cycle length.

and the results evidence that the dynamic behavior of the fuel cell system permits the energy demands from the engine to be instantaneously satisfied by the stack, with only a small contribution from the batteries. Then the role of batteries in this test was mainly that to allow the energy recovery during the regenerative phases, as evidenced by the negative values reached by battery and engine power curves. The effect of this energy recovery is better shown in Fig. 10d, where the battery state of charge is reported versus cycle length. It can be noted that two recharging steps are obtained when the engine operates as generator during the second and fourth deceleration phase of the cycle.

The dynamic behavior of the FCS and dc–dc converter is shown in Fig. 10b, where input and output dc–dc converter powers are monitored during the cycle, together with the hydrogen power, giving a indication of the energy losses before the electric drive.

The energy recovered during regenerative braking was evaluated for both cycles, as percentage of the energy entering the electrical drive, and resulted about 8 and 16% for R47 and R40, respectively.

The instantaneous efficiency of stack and fuel cell system, calculated during both cycles by Eqs. (1) and (2), respectively, are shown in Figs. 11 and 12. According to the results obtained in steady state conditions (Fig. 5) during the phases of low load the stack efficiency is about 0.7, while during the power variations required by the engine it decreases up to the minimum value of about 0.6 in correspondence of the most demanding phase of the cycles, and to about 0.65 at medium load conditions. Regarding the fuel cell system

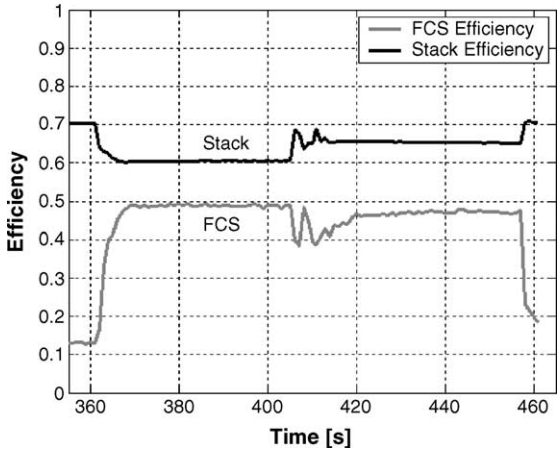

Fig. 11. Stack and fuel cell system efficiency vs. cycle length in load leveled configuration on the R47 driving cycle.

Table 4
Efficiency of the power train and its subsystems during R40 and R47 cycles

	Fuel cell system	dc–dc converter	Electric engine	Power train
Load following (R40 cycle)	0.42	0.78	0.95	0.29
Load leveled (R47 cycle)	0.48	0.86	0.76	0.34

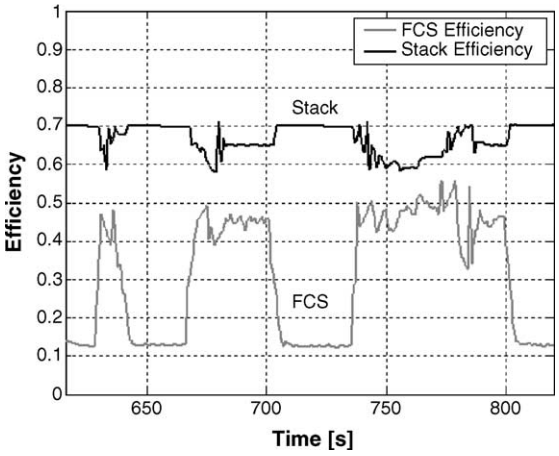

Fig. 12. Stack and fuel cell system efficiency vs. cycle length in load following configuration on the R40 driving cycle.

efficiency, it varies between 0.13 and 0.48 for the R40 cycle (Fig. 12) following the cycle load curve and reproducing the values obtained for each power in steady state conditions (Fig. 5). Then the load following configuration implies that during minimum load phases of the cycle the stack is almost not working, but the system energy losses determine a strong diminution of the instantaneous system efficiency, which negatively affect the average efficiency calculated for the entire cycle. In the load leveled configuration, used for the R47 cycle, the instantaneous system efficiency maintains almost the maximum steady state value for the most part of the cycle length (Fig. 11), so providing a better average efficiency.

The efficiency values obtained for the different components of the power train by experimental measurements on the two cycles are reported in Table 4, as ratio of the integrals of powers on the cycle. The fuel cell system efficiency results higher for the procedure used in R47 cycle ($\eta_{FCS} = 0.48$) with respect to R40 ($\eta_{FCS} = 0.42$), in dependence of different system operative conditions (Figs. 11 and 12). According to the above discussion, during the R47 cycle the stack was controlled to operate in two fixed points, both comprised in the range of high system efficiency (Fig. 5), while during the R40 cycle the stack was left free to follow the load variations, then the fuel cell system in some periods of the cycle worked in low efficiency conditions. The dc–dc converter efficiency on the R47 cycle results slightly higher ($\eta_{dc} = 0.86$) with respect to the value obtained on the R40 cycle ($\eta_{dc} = 0.78$), because of dissipations involved during the transient and low load phases of the load following configuration. The lower efficiency of the electrical drive on the R47 cycle ($\eta_{ED} = 0.76$) with respect to R40 ($\eta_{ED} = 0.95$) can be attributed to the energy losses during the strong acceleration up to engine maximum power during the first phase of the R47 cycle. The total power train efficiency (η_{PT}), calculated by Eq. (4), are reported in the last column of Table 4. The values obtained on the two cycles are affected by the final SOC obtained at the end of the tests. In particular, the final SOC values with respect to the initial ones were lower and higher for R47 and R40 cycle, respectively (Figs. 9d and 10d), then the evaluation of the total efficiency of the power train should take into account the energy necessary to level initial and final SOC for both tests. Assuming to rise the final SOC of R47 test by charging the batteries with the fuel cell system and dc–dc converter, and to diminish the final SOC of R40 by discharging the batteries through the electrical drive, the two efficiency values reported in Table 4 for the power train become both equal to about 0.31.

The data of Table 4 show that the power train efficiency can be mainly affected by the working way of the fuel cell system, through the values of η_{FCS} and η_{dc}, and by the characteristics of the driving cycle, through the values of η_{ED}. The battery efficiency was assumed 100%, but it should be noticed that the interventation of batteries in satisfying power demands was quite limited in both cycles, in particular it was practically negligible for the R40 cycle. This implies that the efficiency evaluations reported in Table 4 would not be significant influenced by battery efficiency, in fact η_{PT} for R47 cycle would result 29 with 80% of battery efficiency and leveled initial and final SOC values, while η_{PT} for R40 cycle would be 30.5% with the same corrections.

Taking in consideration the cycle with minor power requirement (R40), during the which the engine efficiency was higher, and hypothesizing an operative way of the fuel cell system on fixed points characterized by high efficiency, with a limited use of batteries, the evaluations of Table 4 suggest that in some driving conditions a fuel cell power train could reach a total efficiency of about 40%.

A comparison with commercial scooters powered by 50 cm^3 spark ignition engines, made in terms of energy consumption per unit of traveled distance on the same standard driving cycle, evidenced that a very strong reduction of consumed kJ km^{-1} is possible for the fuel cell power train, in particular its overall efficiency resulted about 2.5 times better than conventional propulsion systems.

5. Conclusions

The 2.5 kW fuel cell system characterization evidenced the stack performance and the energy losses associated to the main subsystems. The fuel cell system total efficiency resulted of about 48% in the operative range mainly

used in the experimental runs on cycles (between 500 and 1500 W).

A fuel cell power train of 3.7 kW was realized and coupled to a braking electric machine, allowing the experimental tests to be effected on two different driving cycles, European R47 an R40.

The efficiency of overall propulsion system was determined on both driving cycles, and resulted of about 30%. The efficiency of the individual components of the power train were also analyzed, evidencing the effect of the fuel cell system operative way and of driving cycle power requirements.

The FCS dynamic resulted compatible with variable energy requirements characteristic of the R40 driving cycle investigated.

Acknowledgements

The authors gratefully acknowledge Mr Giovanni Cantilena of Istituto Motori for his cooperation in the setup of the experimental apparatus and execution of the tests.

References

[1] M.H. Fronk, D.L. Wetter, D.A. Masten, A. Bosco, Society of Automotive Engineers, Technical Paper No. 2000-01-0373, 2000.
[2] G. Cacciola, V. Antonucci, S. Freni, J. Power Sources 100 (2001) 67.
[3] B.D. McNicol, D.A.J. Rand, K.R. Williams, J. Power Sources 100 (2001) 47.
[4] M. Conte, A. Iacobazzi, M. Ronchetti, R. Vellone, J. Power Sources 100 (2001) 171.
[5] H.F. Creveling, in: J.M. Norbeck, et al. (Eds.), Hydrogen Fuel for Surface Transportation, Society of Automotive Engineers Inc., Warrendale, PA, USA, 1996, p. 133.
[6] R.J. Potter, T.R. Ralph, D. Thompsett, G.T. Burstein, G.J. Hutchings, Catal. Today 38 (1997) 393.
[7] D.J. Friedman, in: D.J. Holt (Ed.), Hydrogen and its Future as Transportation Fuel, Society of Automotive Engineers Inc., Warrendale, PA, USA, 1999, p. 265.
[8] I.R. Hill, E.E. Andrukaitis, J. Power Sources 103 (2001) 98.
[9] G.W. Vinal, Storage Batteries, John Wiley and Sons Inc., New York, NY, USA, 1955, p. 332.